

## Supporting information

### **GaN:Sn nanoarchitecture integrated on silicon platform for converting CO<sub>2</sub> towards HCOOH by photoelectrocatalysis**

Baowen Zhou, Xianghua Kong, Srinivas Vanka, Shaobo Cheng, Nick Pant, Sheng Chu, Pegah Ghamari, Yichen Wang, Gianluigi Botton, Hong Cuo, and Zetian Mi\*

#### **Experimental section**

**Preparation of GaN NWs/Si.** The n<sup>+</sup>-p silicon junction was firstly fabricated through a standard thermal diffusion process using (100) silicon wafer. Typically, phosphorus and boron as n-type and p-type dopants were deposited on the front and back sides of the polished p-Si (100) wafer by spin-coating. It was then annealed at 900 °C under argon atmosphere for 4 hours. Plasma-assisted MBE was then used for growing GaN NWs on silicon junction under nitrogen rich condition with a N<sub>2</sub> flow rate of 1.0 standard cubic centimeter per minute (sccm). The substrate temperature was 790 °C and the growth duration was ~1.5 h. The forward plasma power was 350 W and the Ga flux was 6×10<sup>-8</sup> Torr.

**Electrodeposition of Sn NPs on GaN NWs/Si.** Sn NPs were deposited on GaN NWs/Si by a simple cyclic voltammetry method. The GaN NWs/Si was immersed into SnCl<sub>2</sub> aqueous solution (200 mL × 1 mmol L<sup>-1</sup>). The electrodeposition was carried out in a PEC chamber by a typical three-electrode configuration, employing Ag/AgCl as reference electrode and Pt as counter electrode. The first depositing step was realized by sweeping potential between +0.1 to +2.0 V, follow by another sweeping deposition at the potential range of -0.5 V to -2.0 V with a desired cycle number. The loading amount and size of Sn is easily tailored by tuning the depositing cycle number. The scanning rate is 100 mV/s. The synthesized sample was thoroughly washed with distilled water after the deposition. Co NPs/GaN NWs/Si and Ni NPs/GaN NWs/Si were fabricated using the same procedure but different precursors. Sn NPs was also electrodeposited on bare silicon substrate without GaN NWs for comparison.

**Characterization of the electrodes.** The TEM work was conducted in the Canadian Centre

for Electron Microscopy in McMaster University. The FEI Titan 80-300-Cube microscope is equipped with a high resolution energy-loss spectrometer (Gatan GIF model 966) with the state-of-the-art K2 Summit Direct Electron Detector Camera. The spectrum image and the HAADF images were acquired with a convergence semi-angle of 19 mrad, and a spectrometer collection semi-angle of 20.7 mrad. The SEM characterization was performed on an Inspect F-50 FE-SEM system. The loading density of Sn supported on GaN nanowire/Si was measured by a Thermo Scientific iCAP 6000 Series inductively coupled plasma-atomic emission spectroscopy instrument. Aqua regia ( $\text{HNO}_3:\text{HCl}=1:3$ ) was used for digesting the samples at 90 °C for 2 hours prior to the testing. XPS was carried out on a Thermo Scientific K-Alpha XPS system with a monochromatic Al  $K\alpha$  source ( $h\nu=1486.6$  eV) at an energy step size of 0.1 eV. The number of energy steps was 211. UV-Vis reflectance spectra analysis was performed on a Cary 5000 UV-Vis-NIR spectrophotometer using a mirror for collecting the baseline.

**Photoelectrochemical reaction.** Photoelectrochemical experiments were carried out in a three-electrode cell. The PEC cell are composed of three compartments including working electrode compartment, reference electrode compartment, and counter compartment, which are separated by Nafion membranes. In the cell, Sn NPs/GaN NWs/Si as well as other photocathodes are used as the working electrode while Pt wire and Ag/AgCl are employed as the counter electrode and the reference electrode, respectively. The electrolyte was 40 mL of 0.1 mol L<sup>-1</sup> KHCO<sub>3</sub> aqueous solution. The electrolyte was purged with CO<sub>2</sub> for at least 10 mins before the reaction. A solar simulator (Oriel LCS-100) was used for light illumination. The light intensity was calibrated to be 100 mW cm<sup>-2</sup>. An Interface 1000E potentiostat (Gamry Instruments) was employed to record the photoelectrochemical data. The analysis of gaseous products was performed by a gas chromatograph with a FID detector (GC 2014, Shimadzu) and a thermal conductivity detector (GC 2010, Shimadzu). The liquid reaction mixtures were studied using 1,3,5-trioxane as an internal standard by nuclear magnetic resonance spectroscopy (NMR 500M, Bruker).

**Calculation of the effective refractive index of the GaN nanowires layer**

$$R_{\text{GaN layer}} = [R_{\text{GaN}} \times FF_{\text{GaN}} + R_{\text{air}} \times (1 - FF_{\text{GaN}})] \quad (1)$$

where  $R_{\text{GaN}}$  the refractive index of GaN is 2.38<sup>[S1]</sup> and  $R_{\text{air}}$  the refractive index of air is 1. Based on the top-view SEM image of GaN NWs/Si,  $FF_{\text{GaN}}$  the fill factor of GaN nanowire arrays aligned on silicon substrate is ~40%.<sup>[S2]</sup>  $R_{\text{GaN layer}}$  is thus calculated to be ~1.5 on the above equation, which is between the index of air (1) and silicon (3.9). Therefore, GaN NWs can act as an efficient anti-reflection coating to improve the optical properties of the silicon substrate, which is consistent with the UV-Vis spectral analysis.

#### Calculation of TON, TOF, and productivity for HCOOH

$$\text{Productivity} = \frac{\text{HCOOH}}{(\text{Surface} \times T)} \quad (2)$$

$$\text{TON} = \frac{\text{HCOOH}}{(\text{Surface} \times LD_{\text{Sn}})} \quad (3)$$

$$\text{TOF} = \frac{\text{HCOOH}}{(\text{Surface} \times LD_{\text{Sn}} \times T)} \quad (4)$$

where  $\text{HCOOH}$  is the amount of formic acid produced in the reaction,  $\text{Surface}$  is the geometric surface area of the working electrode,  $T$  is the reaction time, and  $LD_{\text{Sn}}$  is the

loading density of Sn, which is confirmed by ICP-AES.

## Theoretical section

**Density functional theory calculation.** Density functional theory calculations were performed using the generalized gradient approximation for the exchange-correlation potential, the projector augmented wave method and a plane-wave basis set as implemented in the Vienna ab-initio simulation package.<sup>[S3-S5]</sup> The energy cut-off for the plane-wave basis was set to 500 eV for all calculations. A k-mesh of  $13 \times 9 \times 1$  was adopted to primitive cell of GaN(10  $\bar{1}0$ )-wurtzite and the mesh density of k points was kept fixed when performing calculations related with its supercells. With respect to the geometry structure of  $\text{Sn}_{13}\text{O}_{26}/\text{GaN}(10 \bar{1}0)$ , a  $7 \times 4$  supercell of GaN(10  $\bar{1}0$ ) was used and two different kinds of pseudo hydrogen atoms were employed to passivate the dangling bonds at the bottom of the GaN (wurtzite) slab. The vacuum layer thickness is  $\sim 20 \text{ \AA}$ . In optimizing the system geometry, van der Waals (vdW) interactions were considered by the vdW-DF level with the optB86 exchange functional (optB86-vdW).<sup>[S6]</sup> All structures were fully relaxed until the net force per atom was less than  $0.01 \text{ eV} \cdot \text{\AA}^{-1}$ .

**Table S1. Performance summary of various catalytic architectures for photoelectrochemical  $\text{CO}_2$  reduction into formic acid.**

Catalytic architecture	Condition	Product	TON/TOF $\text{min}^{-1}$	Refs.
Sn NPs/GaN NWs/Si	-0.53 V vs. RHE, 100 $\text{mWcm}^{-2}$ , 10 h	$\text{HCOO}^-$	64000/107	This work
Ru(bpy) <sub>2</sub> dppz-Co <sub>3</sub> O <sub>4</sub> /CA	-0.6 V vs. NHE, 9 $\text{mV} \cdot \text{cm}^{-2}$ Xe lamp, 8h	$\text{HCOO}^-$	978.7/2	S7
InP/[MCE2-A + MCE4]	AM 1.5 G, 24 h, -0.4 V vs. Ag/AgCl	$\text{HCOO}^-$	>17/0.012	S8
SnO <sub>x</sub> NWs/Si	AM 1.5 G, -0.4 V vs. RHE	$\text{HCOO}^-$	-/0.23	S9
[RuCe+RuCA]/CZTSSe	400 < $\lambda$ < 800 nm, 75 times of AM 1.5 G, -0.4 V vs. Ag/AgCl	$\text{HCOO}^-$	7.42/0.041	S0
Mg-CuFeO <sub>2</sub>	470 nm, 2.1 $\text{mW/cm}^2$ , -0.9 V vs. SCE	$\text{HCOO}^-$	-/2 $\times 10^{-5}$	S11

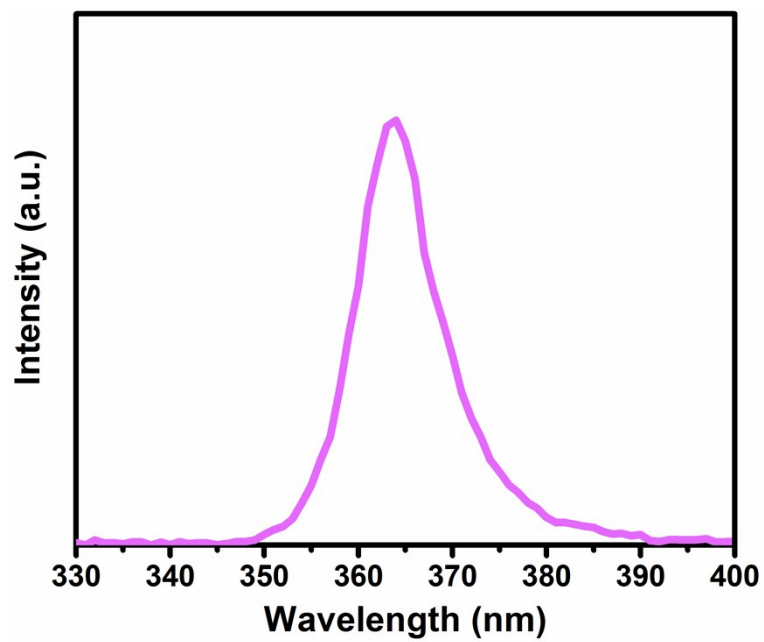


**Figure S1. Photoluminescence emission spectrum of GaN nanowires on silicon.**

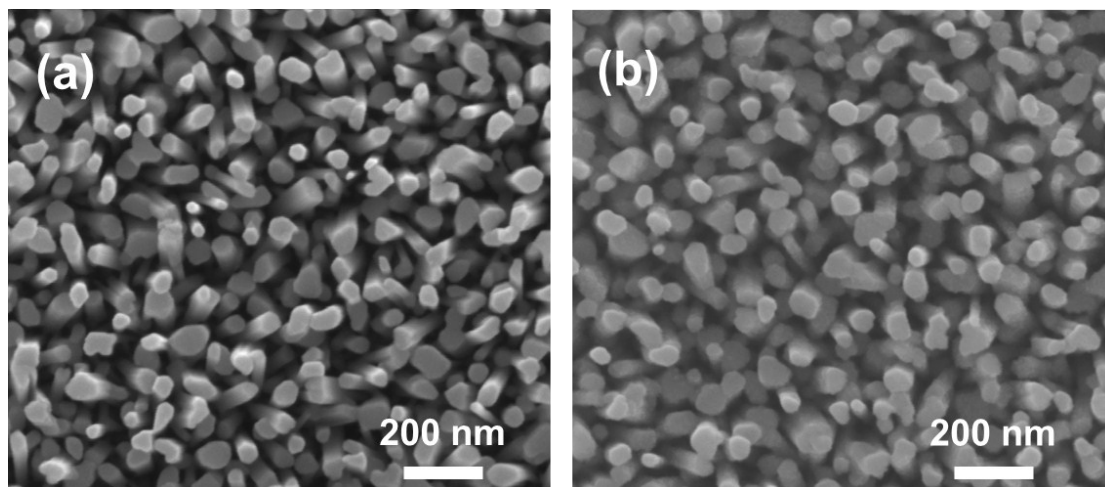


**Figure S2. Top-view SEM images of GaN NWs/Si (a) and Sn NPs/GaN NWs/Si (b).**

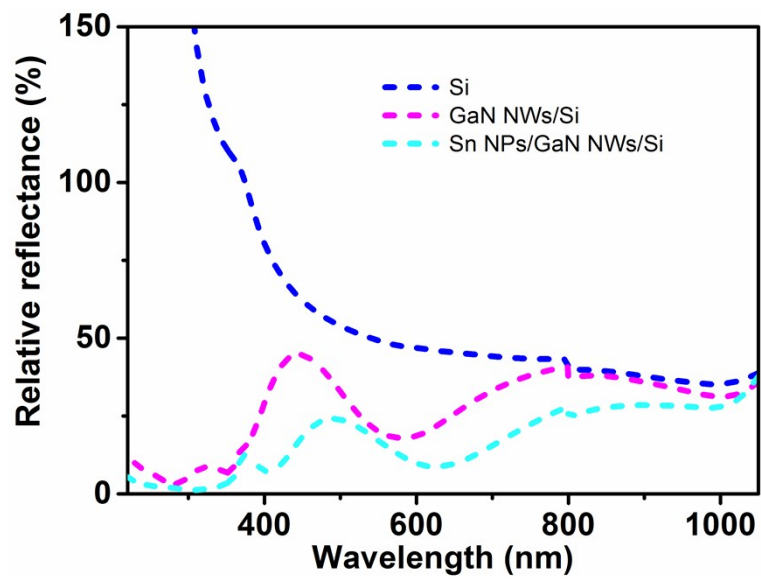
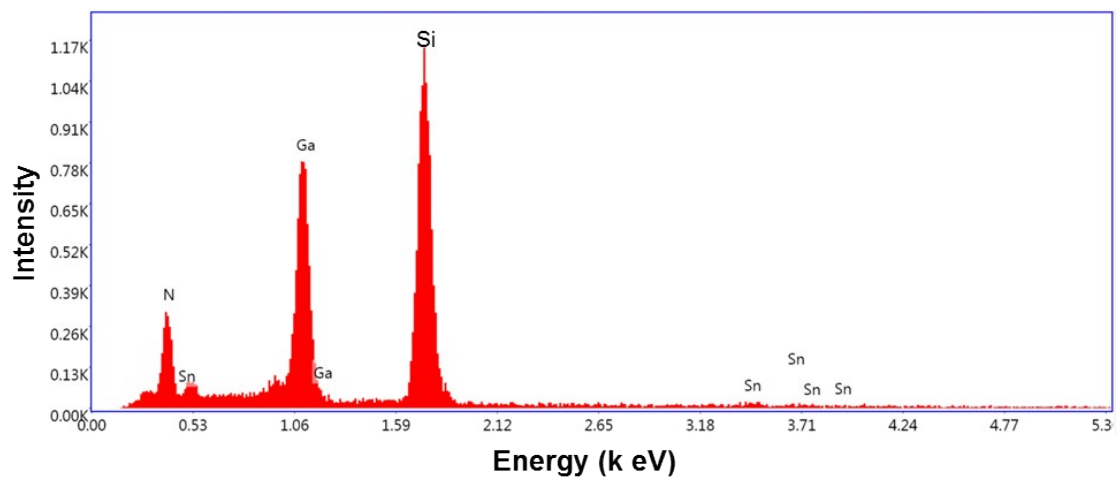
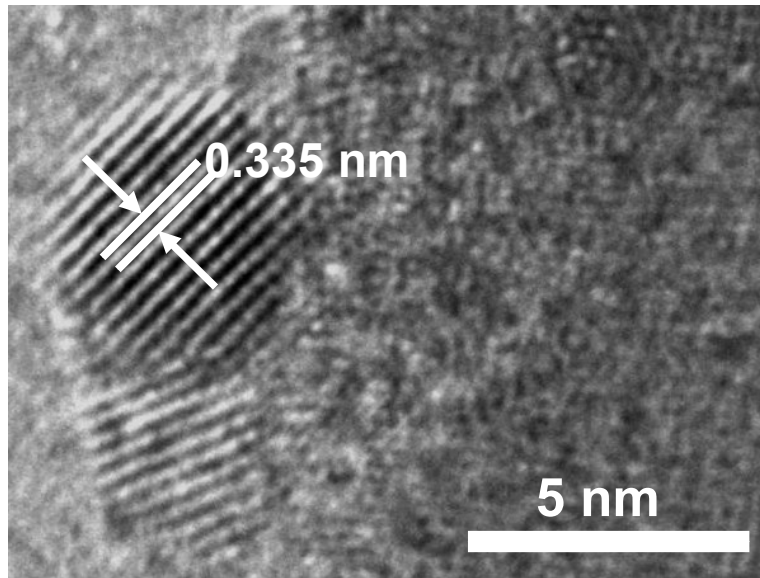


Figure S3. UV-Vis relative reflectance spectra of Si, GaN NWs/Si, and Sn NPs/GaN NWs/ Si.



**Figure S4. Energy dispersive X-ray spectroscopy (EDX) of Sn NPs/GaN NWs/Si.**



**Figure S5. High-resolution TEM image of Sn NPs supported on GaN nanowires.**

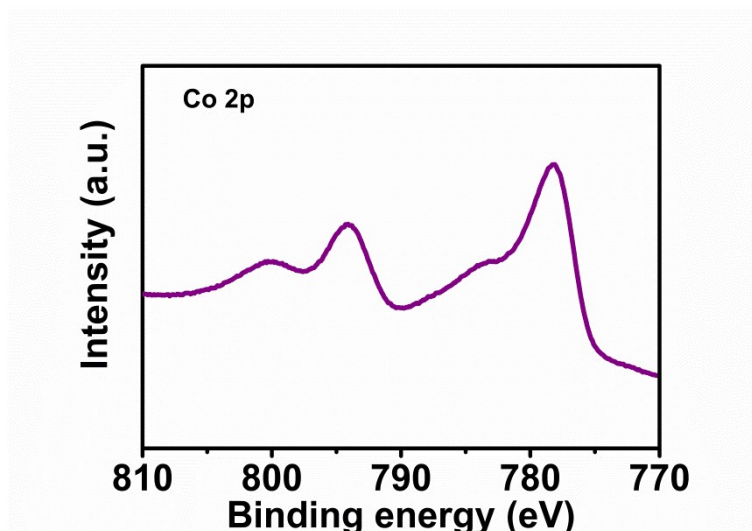
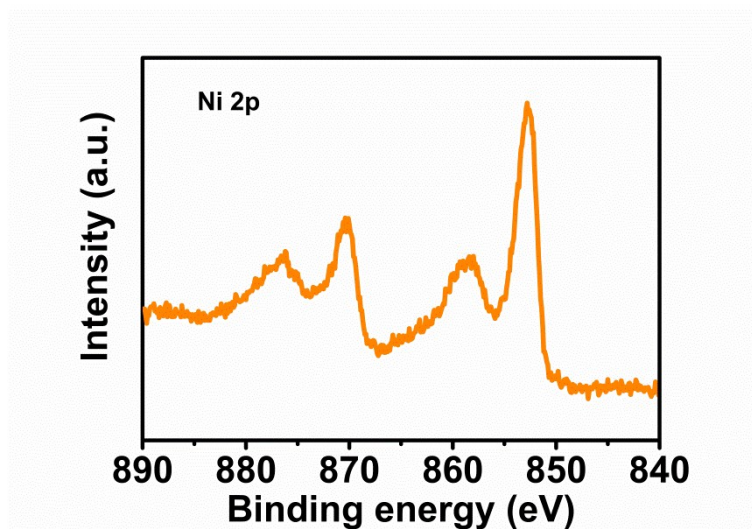


Figure S6. X-ray photoelectron spectroscopy of Co NPs over Co NPs/GaN

NWs/Si



**Figure S7. X-ray photoelectron spectroscopy of Ni NPs over Ni NPs/GaN NWs/Si.**

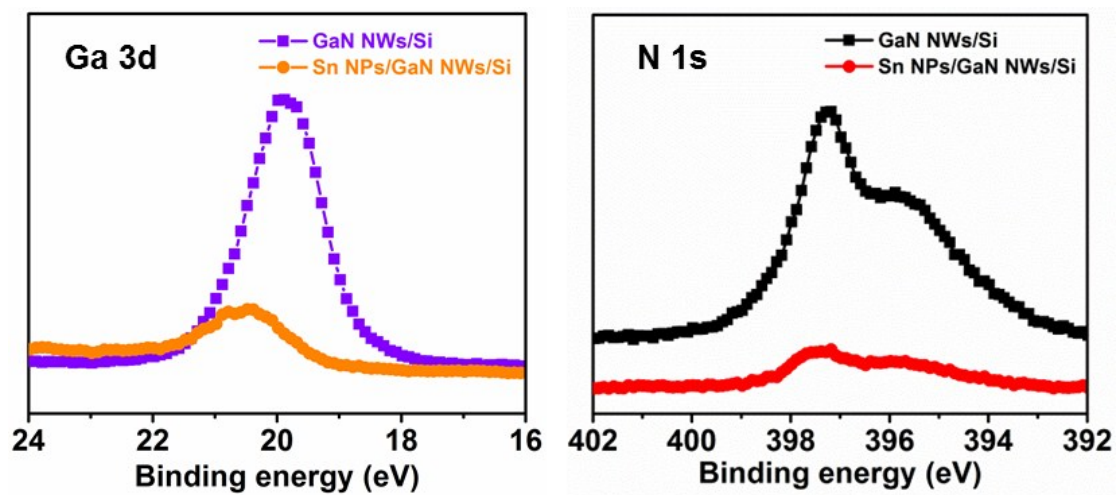
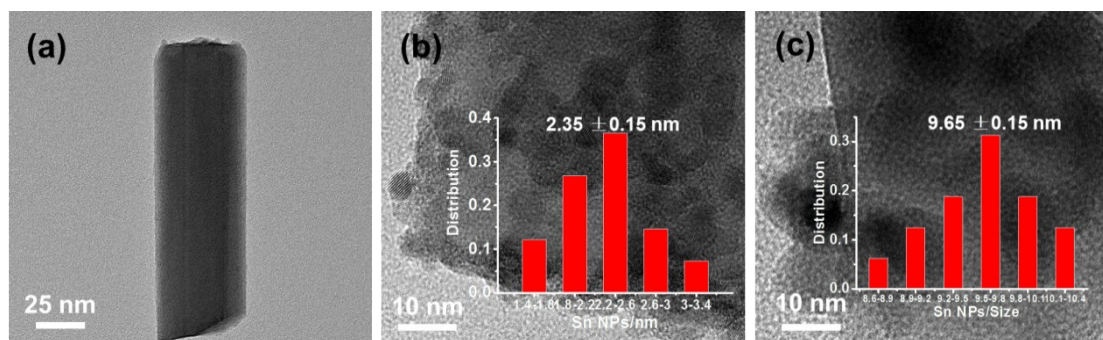
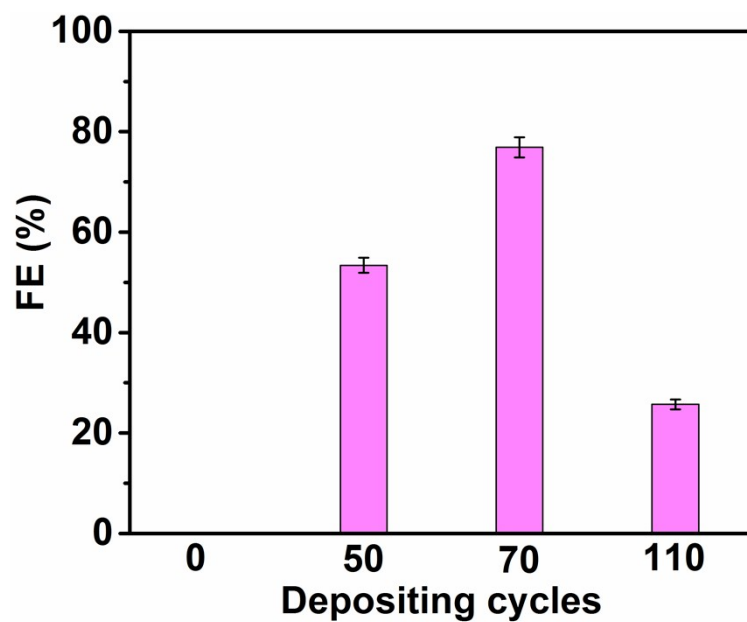


Figure S8. Binding energies of Ga 3d (left) and N 1s (right) in GaN NWs/Si and Sn NPs/GaN NWs/Si.



**Figure S9. TEM images of Sn NPs/GaN NWs/Si with different Sn NPs depositing cycles. (a) 0 cycle, (b) 70 cycles, (c) 110 cycles.**



**Figure S10.** FE for HCOOH production of Sn NPs/GaN NWs/Si with various depositing cycles of Sn NPs in CO<sub>2</sub>-purged 0.1 M KHCO<sub>3</sub> under standard one-sun illumination at -0.53 V vs. RHE.

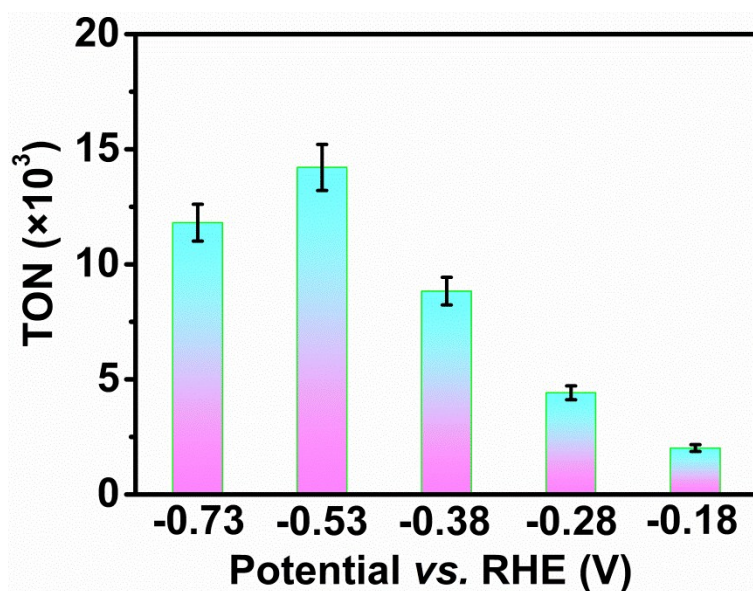


**Figure S11.** Influence of the applied potential on the turnover number of Sn NPs/GaN NWs/Si for formic acid formation in  $\text{CO}_2$ -purged 0.1 M  $\text{KHCO}_3$  under standard one-sun illumination for 2 hours.

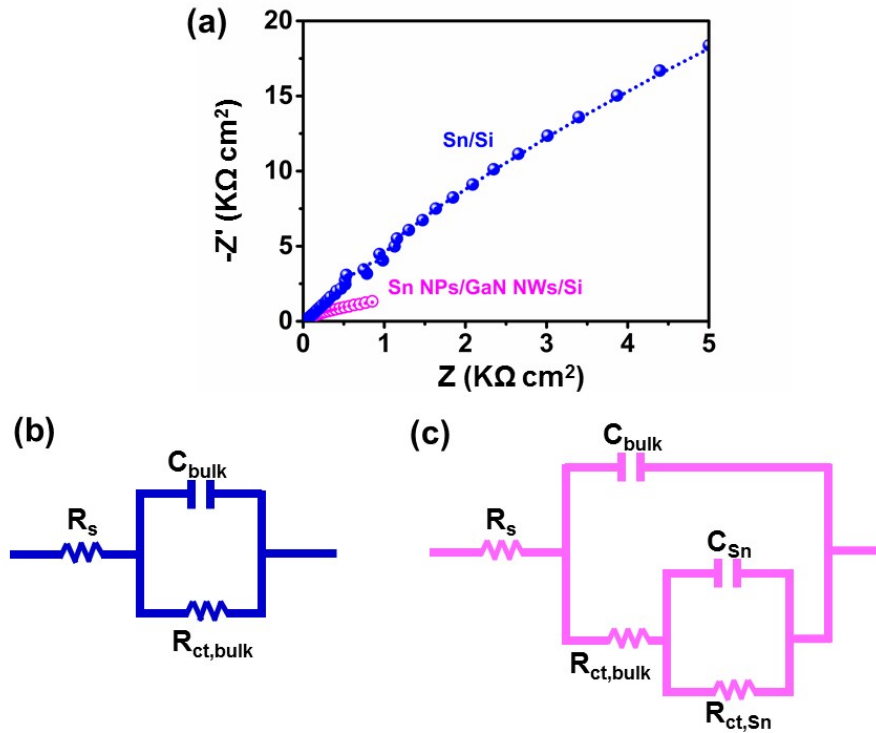


**Figure S12. Electrochemical impedance spectroscopy of Sn/Si and Sn NPs/GaN NWs/Si in  $\text{CO}_2$ -purged 0.1 M  $\text{KHCO}_3$  aqueous solution under standard one-sun illumination (a). The fitting equivalent circuits of Sn/Si (b) and Sn NPs/GaN NWs/Si (c) are illustrated for the interpretation of the electrochemical impedance spectroscopy. A series resistance of  $R_s$  includes the band bending within  $n^+$ -p silicon junction and the band bending between  $n^+$ -Si and  $n^+$ -GaN.  $C_{\text{bulk}}$  represents a constant phase element (CPE) for the bulk semiconductor with electrolyte in the equivalent circuit.  $R_{\text{ct,bulk}}$  represents a charge transfer resistance from semiconductor conduction band.  $R_{\text{ct,Sn}}$  signifies a charge transfer resistance of electron from Sn NPs to the electrolyte.  $C_{\text{Sn}}$  is a CPE for Sn.**

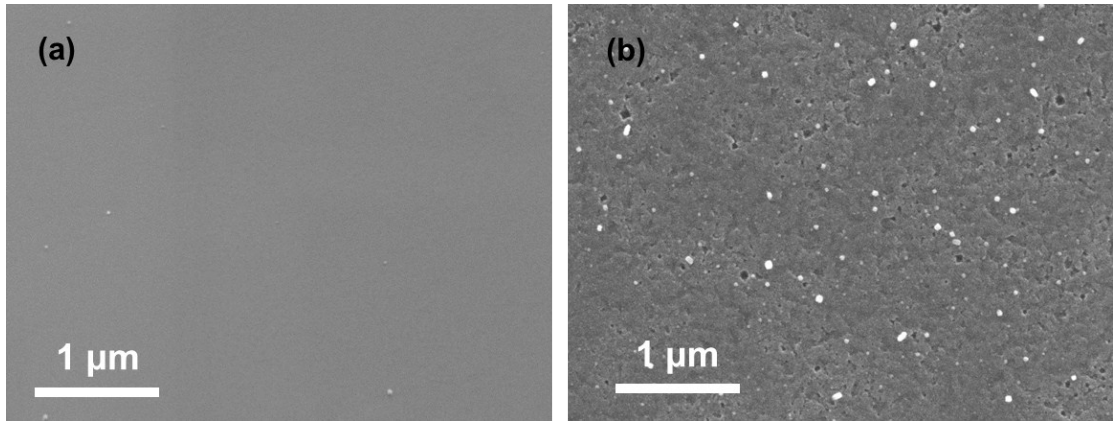


**Figure S13. SEM images of bare Si and Sn/Si.**

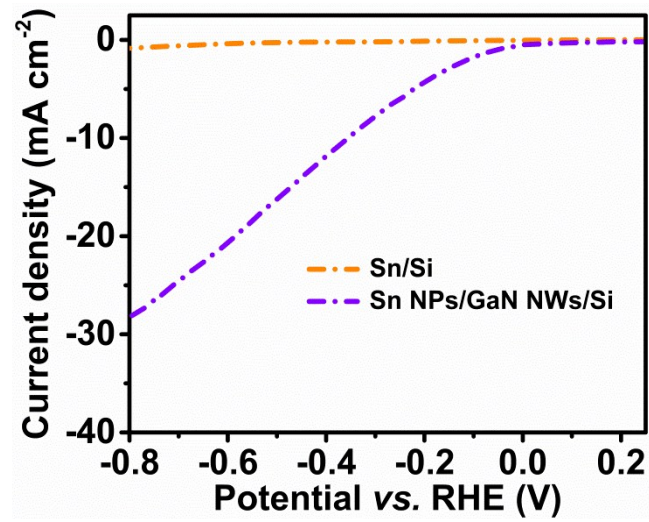


**Figure S14.  $J$ - $V$  curves of Sn/Si and Sn NPs/GaN NWs/Si in CO<sub>2</sub>-purged 0.1 M KHCO<sub>3</sub> aqueous solution under standard one-sun illumination.**

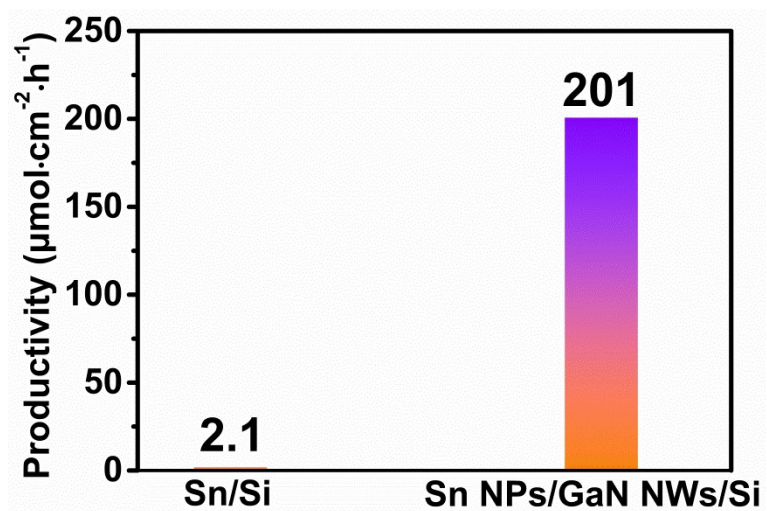


**Figure S15.** The productivity of Sn/ Si and Sn NPs/GaN NWs/Si in  $\text{CO}_2$ -purged 0.1 M  $\text{KHCO}_3$  aqueous solution under standard one-sun illumination. Inset is the magnification of the original figure to show the productivity of Sn/Si.

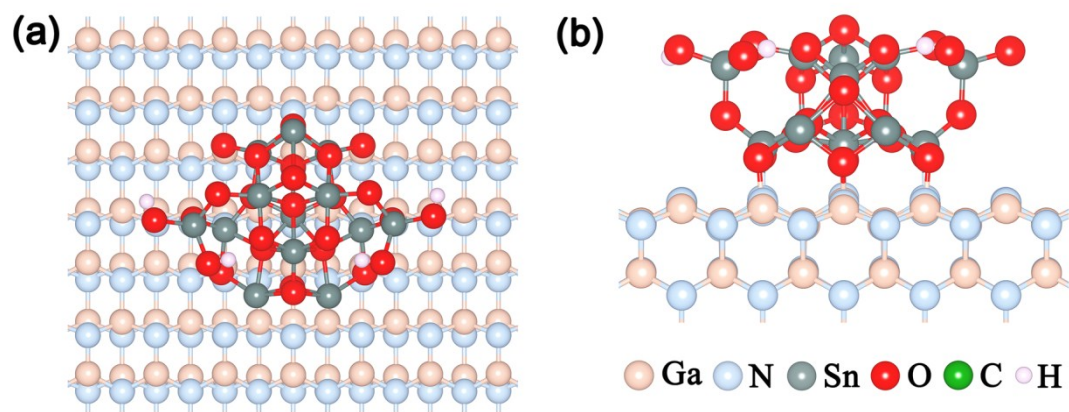


**Figure S16.** (a) Top and (b) side views of the optimized geometry of  $\text{Sn}_{13}\text{O}_{26}/\text{GaN}(10\bar{1}0)$  system. The hydroxylation was applied in the calculations due to the effect of PEC  $\text{CO}_2$  reduction conditions in an aqueous environment.

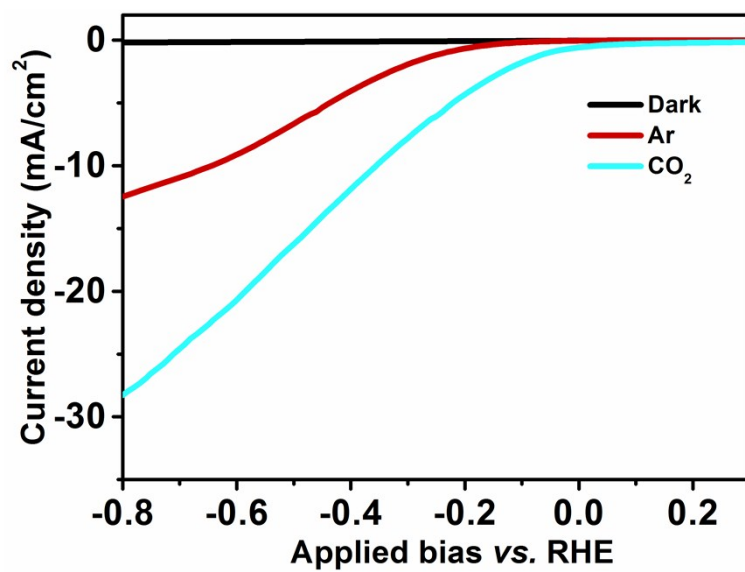
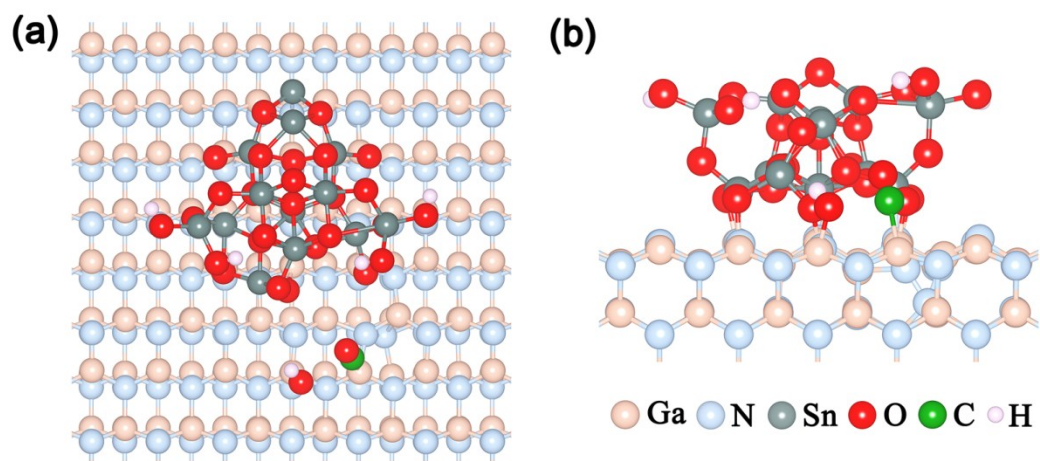
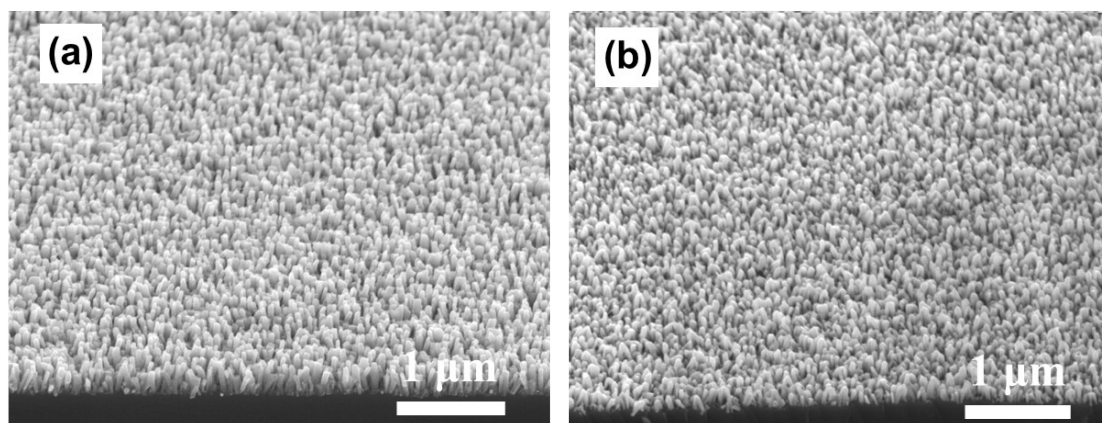


Figure S17. *J-V* curve of Sn NPs/GaN NWs/Si in 0.1 M KHCO<sub>3</sub> aqueous solution under different atmosphere.



**Figure S18. (a) Top and (b) side views of the most energetically stable and fully relaxed \*OH adsorption configuration on the \*CO/Sn<sub>13</sub>O<sub>26</sub>/GaN(10 $\bar{1}$ 0) system.**

Sn: grey, O: red, C: green, N: light blue, Ga: light brown and H: light pink.



**Figure S19. SEM images of Sn NPs/GaN NWs/Si before (a) and after (b) 10 hours reaction at a fixed potential of -0.53 V vs. RHE under standard one-sun illumination.**

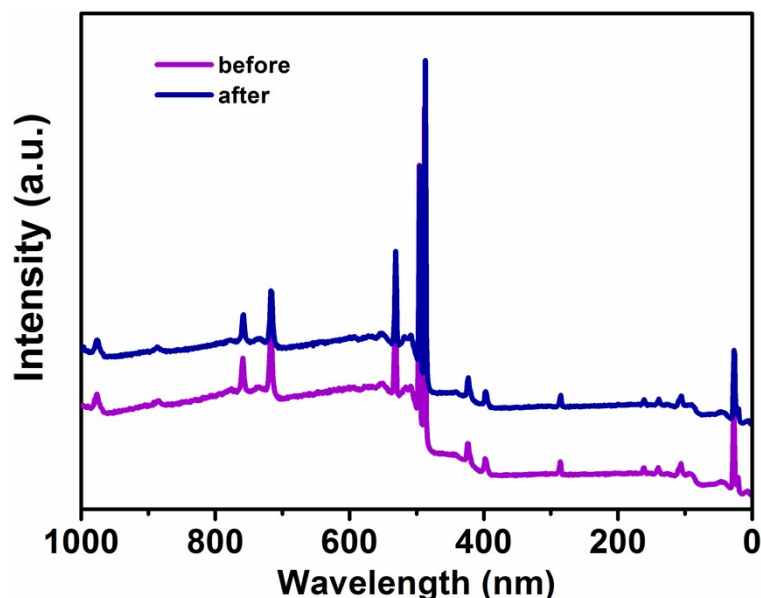


**Figure S20.** XPS Spectra of Sn NPs/GaN NWs/Si before (a) and after (b) 10 hours reaction at a fixed potential of -0.53 V vs. RHE under standard one-sun illumination.

## References

- [S1] A. S. Barker, J. M. Heger. *Phys. Rev. B* **1973**, 7, 743-750.
- [S2] S. Chu, S. Z. Fan, Y. J. Wang, D. Rossouw, Y. C. Wang, G. A. Botton, Z. T. Mi. *Angew. Chem. Int. Ed.* **2016**, 55, 14262-14266.
- [S3] P. E. Blochl. *Phys. Rev. B* **1994**, 50, 17953-17979.
- [S4] G. Kresse, D. Joubert, *Phys. Rev. B* **1999**, 59, 1758-1775.
- [S5] G. Kresse, J. Furthmuller. *Phys. Rev. B* **1996**, 54, 11169-11186.
- [S6] J. Klimes, D. R. Bowler, A. Michaelides. *Phys. Rev. B* **2011**, 83, 195131.
- [S7] X. F. Huang, Q. Shen, J. B. Liu, N. J. Yang, G. H. Zhao. *Energy Environ. Sci.* **2016**, 9, 3161-3171.
- [S8] S. Sato, T. Arai, T. Morikawa, K. Uemura, T. M. Suzuki, H. Tanaka, T. Kajino. *J. Am. Chem. Soc.* **2011**, 133, 15240-15243.
- [S9] K. R. Rao, S. Pishgar, J. Strain, B. Kumar, V. Atla, S. Kumari, J. M. Spurgeon. *J. Mater. Chem. A.* **2018**, 6, 1736-1742.
- [S10] T. Arai, S. Tajima, S. Sato, K. Uemura, T. Morikawa, T. Kajino. *Chem. Commun.* **2011**, 47, 12664-12666.

[S11] J. Gu, A. Wuttig, J. W. Krizan, Y. Hu, Z. M. Detweiler, R. J. Cava, A. B. Bocarsly. *J. Phys. Chem. C* **2013**, 117, 12415-12422.

### **Author Contributions**

B.Z. and Z.M. designed this work. B.Z. performed the electrodeposition, photoelectrochemical experiments, photoelectrodes characterization, and analyzed the results. X. K. and H. G. proposed and carried out the density functional theory (DFT) calculations as well as the analysis of the results. B.Z. joined the DFT discussion. The preparation of the n<sup>+</sup>-p Si junction and MBE growth of GaN NWs were conducted by S.V. S.C. and G.B. performed the STEM-HAADF characterization. N.P. S.C. P.G. and Y.W. made some contribution to characterization studies and data analysis. B.Z., X. K., H. G. and Z.M. wrote the manuscript with contributions from other co-authors.